Proceedings World Geothermal Congress 2020+1
Reykjavik, Iceland, April - October 2021

Geothermal Favorability Assessment of the Gediz Graben Through Correlation and GIS Based MCDA Methodologies

Selim Cambazoğlu[1], Gözde Pınar Yal[1], Arif Mert Eker[2], Osman Şen[2], Haluk Akgün[1]

[1] Geotechnology Unit, Department of Geological Engineering, Middle East Technical University, Ankara, Turkey

[2] SDS Energy, Ankara, Turkey

selimcambaz@gmail.com

Keywords: GIS, MCDA, Western Anatolia, geothermal favorability, Gediz Graben, bivariate correlation

ABSTRACT

Turkey is ranked fourth in the world in terms of geothermal production with more than 45 active plants having 1347 MWe installed capacity. Western Anatolia, primarily the Büyük Menderes Graben followed by the Gediz Graben, are among the most important regions in the world in terms of geothermal energy potential and hosts almost the entire installed capacity of Turkey. There are several operational geothermal power plants in the Gediz Graben where other projects are either in a construction or planning stage. Following the preliminary exploration, one of the most important stages in a geothermal project is well site selection due to high drilling costs. GIS has been proven to be a useful tool in identification of potential areas for detailed resource exploration through detection of spatial correlations between various types of data that have been collected during the initial exploration stages.

In this study, various geothermal potential and favorability criteria layers were generated, and each layer was incorporated into a GIS environment. These variable layers were correlated with a favorability map generated based on knowledge driven criteria ranking in order to assess the relative importance of each criterion. A MCDA (Multi-Criteria Decision Analysis) was performed to generate a geothermal favorability map of the region. Finally, the success rate of the final geothermal favorability map was assessed based on the known producing wells.

1. INTRODUCTION

Büyük Menderes and Gediz Grabens are the two major regions in Western Anatolia generating almost entire geothermal power in Turkey. The total geothermal installed capacity of Turkey is 1347 MWe and Gediz Graben hosts nine operational geothermal power plants in the Gediz Graben with a total installed capacity of 215 MWe and there are several projects in planning and construction stage with more than 300 MWe possible installed capacity.

In this study, the favorability map of the region which was generated according to knowledge based ranking of criteria layers related with geothermal potential and favorability (Cambazoğlu et al., 2019) was correlated with the each criteria based on Pearson Correlation. The relative importance of each layer was then rearranged according to the results of the statistical analysis and a favorability map was generated based on this new ranking and weight assignment. Both maps were correlated with the known geothermal producing wells and their results were discussed.

Topographical, geological, hot spring location, active fault map, Bouger gravity anomaly map, earthquake epicenter catalogue, Landsat and ASTER satellite images were used to generate slope, Normalized Difference Vegetation Index (NDVI), Gutenberg-Richter b-value, fault density, distance to fault, distance to graben center, Neogene cap rock, ASTER night-time surface temperature data and distance to hot springs layers to be used as criteria maps in the assessment. A MCDA (Multi-Criteria Decision Analysis) was performed by using TOPSIS (Technique for Order Preference by Similarity to the Ideal Solution) methodology based on each ranking and it was observed that knowledge based relative importance ranking have presented better results in comparison to datasets ranked based on the results of the bivariate correlation.

2. STUDY AREA AND GEOLOGICAL SETTING

The study area is located at N-S extending Western Anatolia and within the Gediz Graben having an WNW-ESE arc-shape trend with 140-150 km length and 10 to 40 km width bounded by Bozdağ Mountains and a series of ENE-WSW trending horst-graben systems from south and north, respectively. (Yılmaz et al., 2000; Bozkurt and Sözbilir, 2004, Klingel et al., 2015) (Figure 1). There are different models regarding the extensional regime in the Aegean Extensional Province, however, it is generally accepted that the extension has initiated in southwest Turkey by the latest Oligocene - Early Miocene time and has led to the formation of the Miocene metamorphic core-complex and Plio-Quaternary grabens (Çiftçi and Bozkurt, 2009). The Menderes Massif is divided into sub-massifs by Gediz and Büyük Menders grabens which are bound by large scale detachment faults respectively from south and north, forming the two regions with the highest geothermal potential in Western Anatolia (Bozkurt and Sözbilir, 2004; Çiftçi and Bozkurt, 2009; Gessner et al., 2013).

The southern margin of the asymmetric Gediz Graben is seismically more active with presently a low-angle (˜10°) detachment fault and cross-cutting high angle north dipping normal faults whereas, the northern margin has less pronounced topography and inactive high angle normal faults. The low-angle detachment fault has formed an unconformity between the pre-Neogene crystalline basement and Miocene to recent graben-fill units (Yilmaz et al., 2000; Sözbilir, 2002; Çiftçi and Bozkurt, 2009, 2010). The Paleozoic-Mesozoic aged basement Menderes Metamorphics are composed of granitic augen-gneiss, various gneisses, metavolcanics and metasedimentary units. The metasedimentary units of Paleozoic-Early Tertiary age are moderate to low degree metamorphosed schist, quartz- schist, calc-schist and marbles. The basement Menderes Massif is unconformably overlain by the Neogene Alaşehir Group composed of continental clastics and carbonate rock units which is unconformably overlain by Miocene-

Pliocene aged Kızıldağ Group composed of clastic units. The Plio-Quaternary Sart Group, composed of conglomerates with minor sandstone and clays, unconformably overlays the Miocene-Pliocene sequence and is overlain by the Quaternary alluvial deposits (Yılmaz et al., 2000) (Fig. 2). The Paleozoic-Mesozoic Menderes Metamorphics serve as the reservoir rocks of the geothermal system whereas the Neogene rock units serve as the cap rock of the geothermal system in the region (Yılmazer et al., 2010).

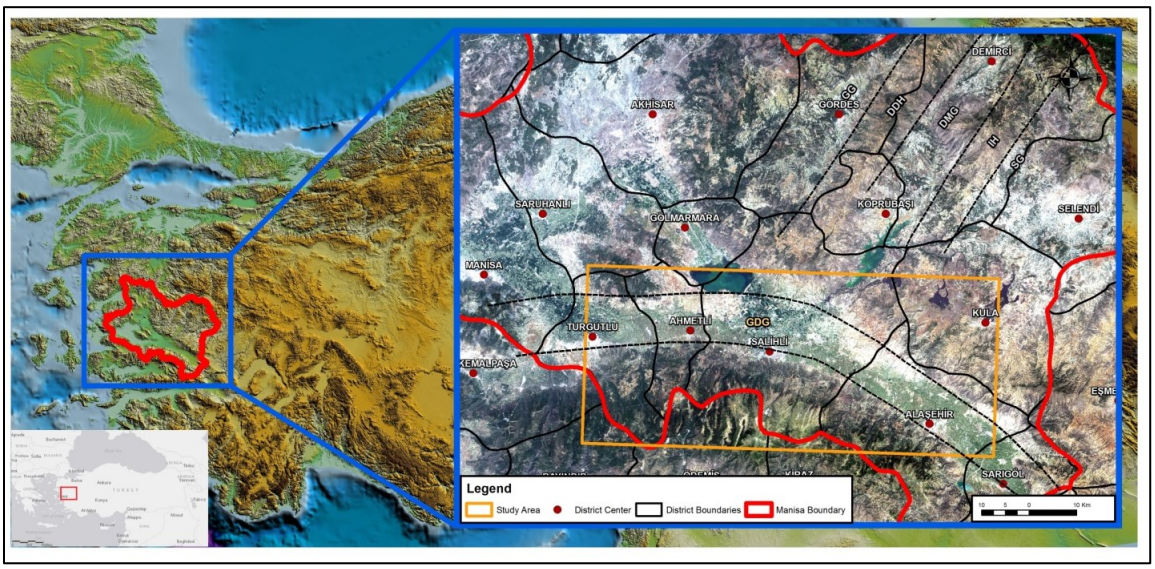

Figure 1. Location map showing the extent of the confined study area in blue color boundary over true color Landsat image (GDG: Gediz Graben, GG: Gördes Graben, DDH: Dilekdağ-Demircidağ Horst, DG: Demirci Graben, IH: Icikler Horst, SG: Selendi Graben).

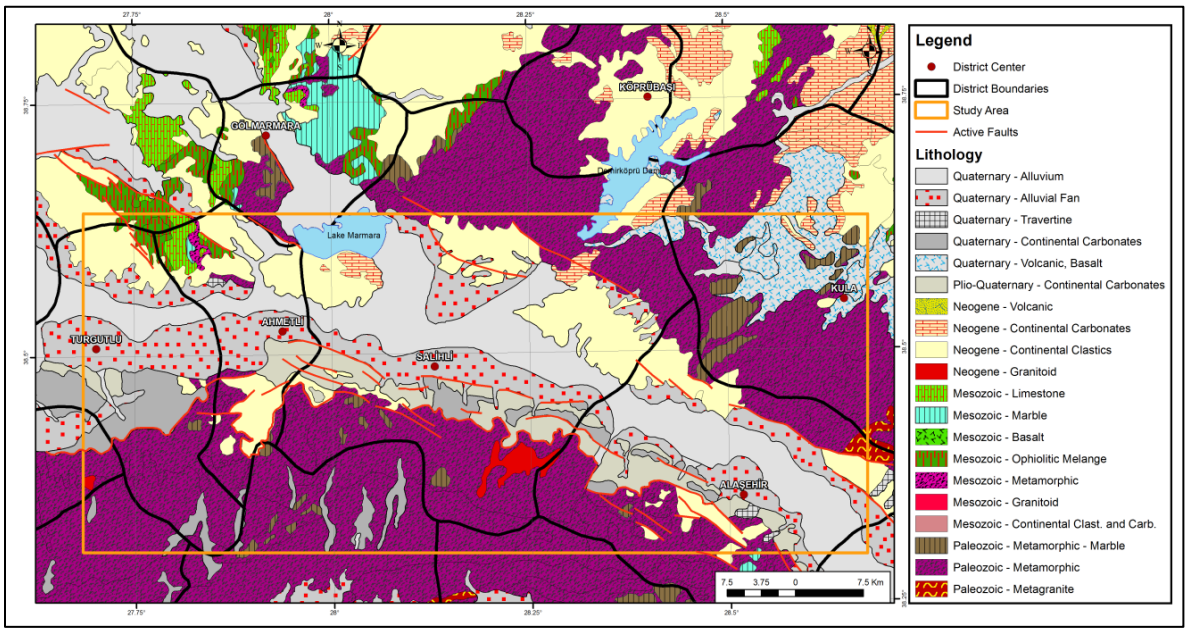

Figure 2. Generalized geological map of the study area and its surroundings (Adapted from: MTA, 2002).

3. DATASETS AND CRITERIA LAYERS

In order the assess the geothermal favorability of the Gediz Graben, 9 criteria layers were generated from different datasets (Table 1). These criteria layers included fault density and distance to fault, distance to hot springs, distance to cap rock units and graben center, night-time surface temperature, b-value, slope angle and NDVI.

The presence of faults is directly related with the fracture network generation at the reservoir level and heat transport from depth especially in the case of southern bounding crustal scale detachment fault. Therefore, distance to faults and more importantly fault density layer which was included to account for the importance of cross-cutting relationship at the southern margin of the graben were prepared in order to represent both proximity to the possibly fractured lithologies and the presence of a highly fractured reservoir. Initially, a generalized fault map was compiled by digitizing different fault maps in the literature (MTA, 2002; Bozkurt and Sözbilir, 2004; Çiftçi and Bozkurt, 2009; Yılmazer et al., 2010; Duman et al., 2011; Gessner et al., 2013; Klingel et al., 2015).

Table 1. Datasets and criteria maps used in the study.

Dataset	Criteria maps	Source
Hot spring	Distance to hot springs	Akkuş et al., 2005
Fault map	Fault density	MTA,2002; Bozkurt and Sözbilir, 2004; Çiftçi and Bozkurt, 2009; Yılmazer et al., 2010; Duman et al., 2011; Gesner et al., 2013; Klingel et al., 2015
	Distance to fault	
LANDSAT	Vegetation-NDVI	USGS-EROS, 2017
ASTER-TIR	Night-time surface temperature	NASA LP DAAC, 2017
DEM	Slope angle	General Command of Mapping, 2000
Geological map	Neocene cap rock	MTA, 2002
Regional geophysical data	Distance to graben center	Arslan et al., 2010; Çiftçi and Bozkurt, 2010
Earthquake epicenter	Gutenberg-Richter b-value	KOERI, 2017

The distance to fault layer was generated by using Euclidian distance to fault lines and the values of the resultant layer (30 m x 30 m resolution) ranging between 0 and 17.73 km with a mean value of 3.5 km. For the fault density map, a search radius was identified based on 9 km average depth of the earthquake epicenters within the study area (KOERI, 2017) and by considering the dip-angle of the faults within the study area based on focal mechanism solutions where dip angle values range between 28° and 89° with a mean value of 60° (Shah, 2015). Therefore, the search radius for the fault density map was identified as 5.2 km and generated according to Kernel density approach as described by Silverman (1986) by considering a weight factor of 2 for the detachment fault trace. Both distance to fault and fault density layers (Figure 3 and 4, respectively) were generated in 30 m resolution.

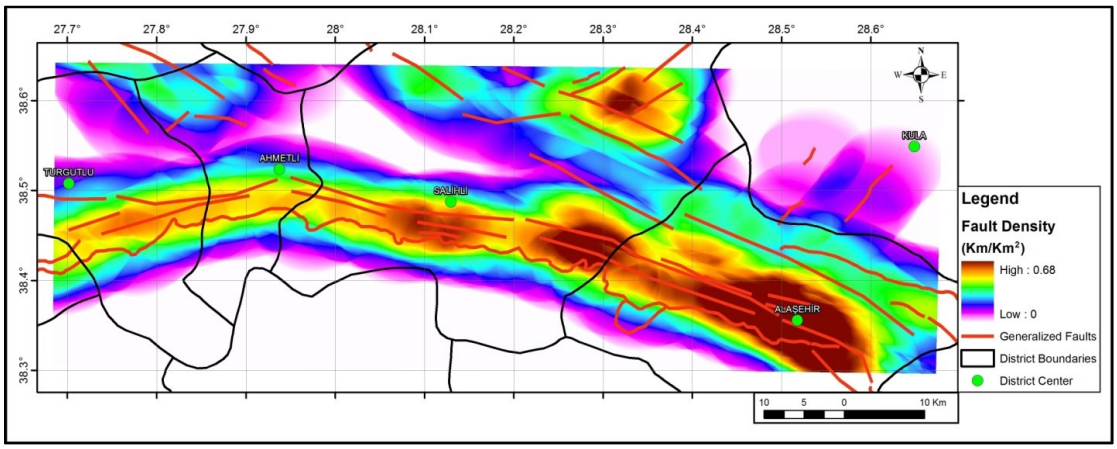

Figure 3. Fault density map of the study area (Generalized fault lines are shown in red).

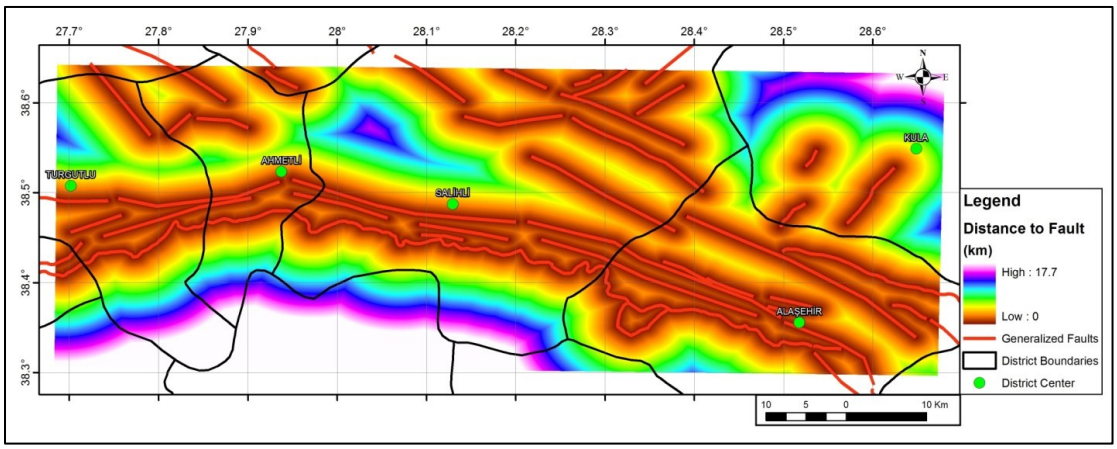

Figure 4. Distance to fault map of the study area (Generalized fault lines are shown in red).

The distance to hot springs and cap rock units layers are directly related with the geothermal system. As hot springs are spatially location specific digitized from Akkuş et al. (2005), this criterion was included as a distance layer by using Euclidian distance with a resolution of 30 m (Figure 5). The cap rock of the geothermal system in the Gediz Graben region is the Miocene units unconformably overlying the pre-Neogene basement Menderes Massif (Yılmazer et al., 2010). Therefore the digitized 1:500.000

scale geological map (MTA, 2002) is divided into two as pre- and post-Neogene units and a distance to post-Neogene unit layer was generated with a resolution of 30 m (Figure 6). Furthermore, since the cap rock thickness is another important parameter for geothermal occurrence, the distance to the graben center map was prepared in order to represent the decreasing thickness of the cap rock units away from the center of the graben as identified from 1:1250000 scale regional geophysical maps (free air gravity and Bouger gravity maps) (Arslan et al., 2010), 1:500000 scale geological map (MTA, 2002) and seismic reflection interpretations of Çiftçi and Bozkurt (2010). The Euclidian distance map (Figure 7) was generated by using a weight factor of 0.5 for the southern section of the graben due to the following reasons: 1) most of the known geothermal hot springs are located at the southern part of the graben, 2) the southern margin is known to be more active from a seismicity standpoint, 3) the southern margin that is bound by low angle detachment fault is cross-cut by the high angle north dipping normal faults, and 4) thinning of Miocene cap rock from south to north.

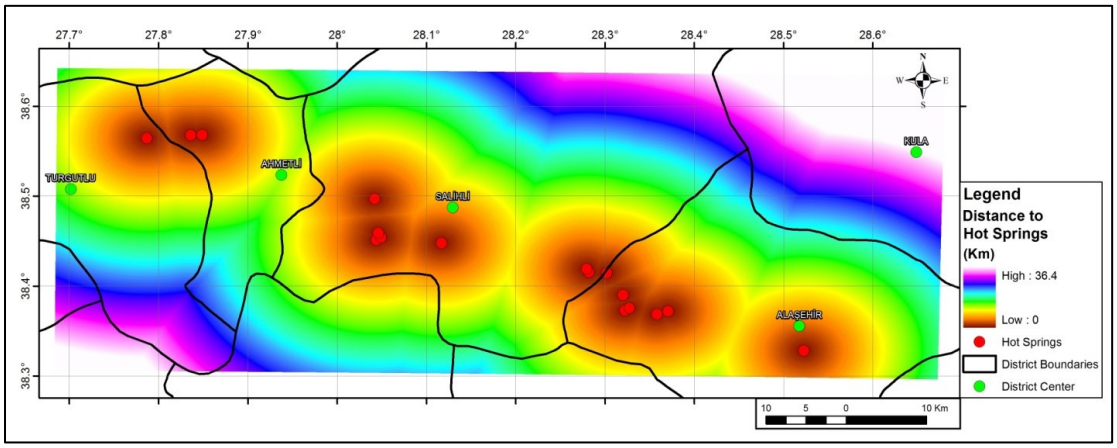

Figure 5. Distance to hot spring map of the study area (Hot springs shown as red dots).

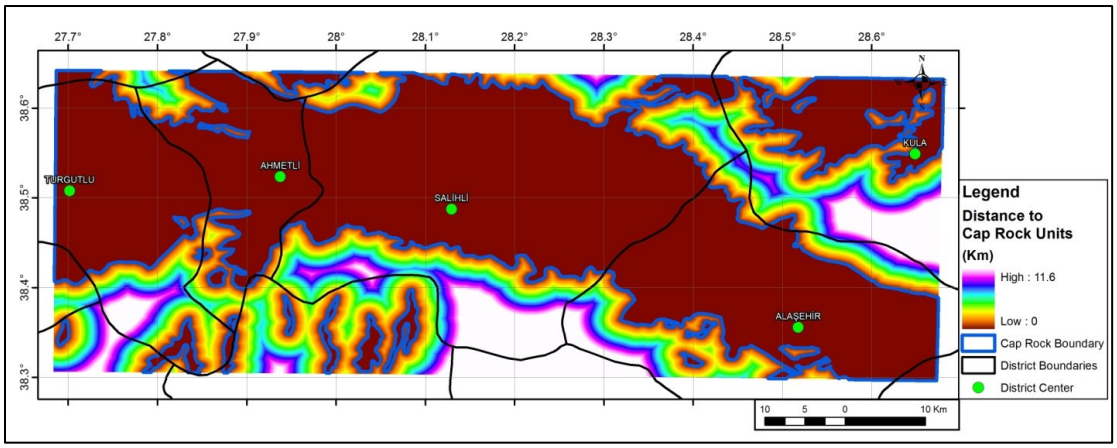

Figure 6. Distance to cap rock units (Cap rock unit boundaries shown as blue lines).

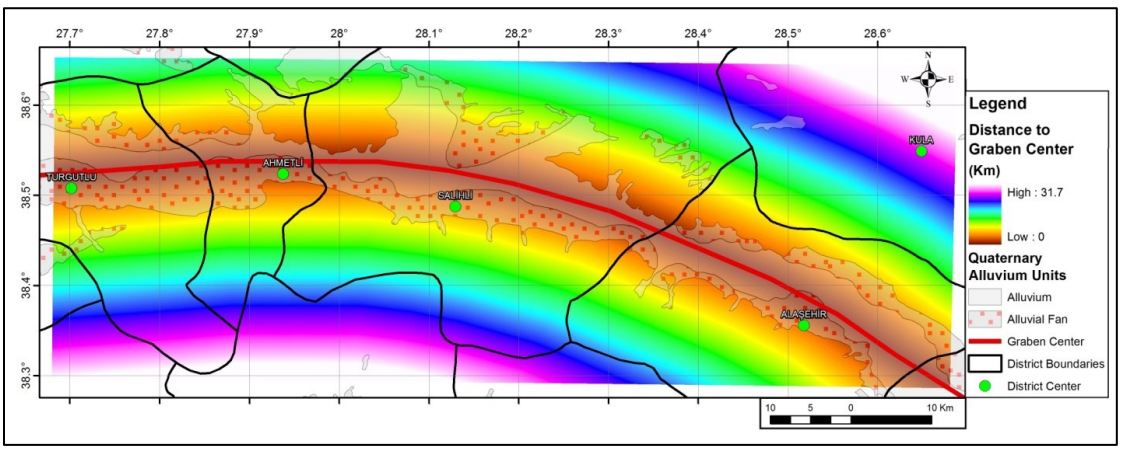

Figure 7. Distance to graben center.

The night-time surface temperature layer was generated by using ASTER L1T satellite image data (NASA LP DAAC, 2015), courtesy of the NASA Land Processes Distributed Active Archive Center (LP DAAC), USGS/Earth Resources Observation and Science (EROS) Center, Sioux Falls, South Dakota. A total of 6 ASTER images were used mainly from August 2013 and from September 2012 as a 5 km filler. Surface temperature image was generated by applying emissivity and temperature separation algorithm (Hook et al., 1992; Gillespie et al., 1998) on the five thermal infrared (TIR) bands of ASTER images. Elevation correction was applied by considering -5.15°C/km environmental lapse rate estimated according to linear regression between night-time surface temperature and elevation data with an R^2 value of 0.74 (Eneva and Coolbaugh, 2009; Gutierrez et al., 2012). The Digital Elevation Model (DEM) with 30 m resolution generated from the 1:25000 scale topographical map contours was used for the elevation correction to obtain the final surface temperature image (Figure 8).

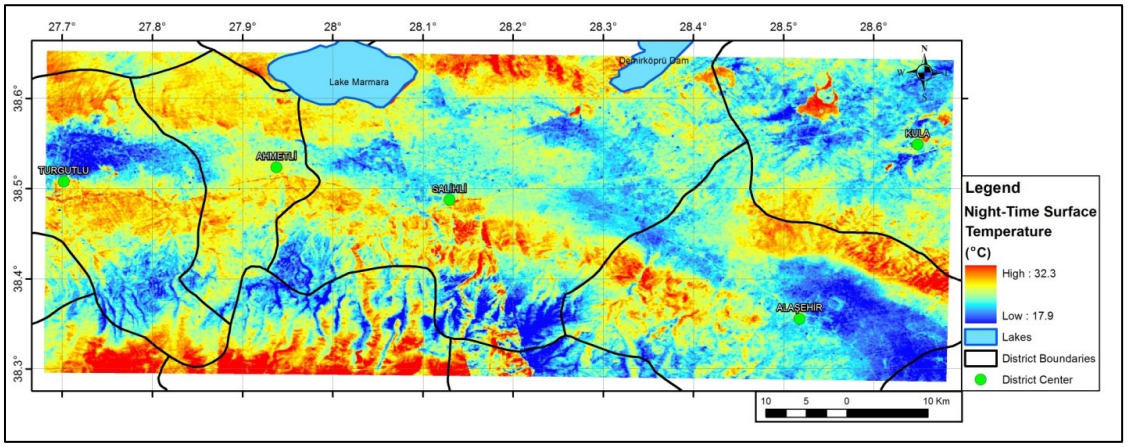

Figure 8. Night-time surface temperature map.

Along with the fault density and distance to fault maps, the Gutenberg-Richter (1949) b-value map which is directly related to earthquake occurrence and was used to explain the seismo-tectonic character of the region. The b-value was calculated according to magnitude-frequency recurrence relation of $\log_{10}N(M) = a + b(M)$ as proposed by Gutenberg and Richter (1949) where, N is the number of earthquakes with a magnitude equal to or larger than M, and 'a' and 'b' are the regression coefficients. The epicenter data of the region that was compiled by the Kandilli Observatory and Earthquake Research Institute (KOERI, 2017) was used as an input for the Z-Map seismic analysis software (Weimer, 2001). In order to generate a seamless b-value map, a search radius of 45 km was selected by considering the maximum earthquake depth of 120 km that was observed in the region and more importantly, direct seismicity relationship that was observed along the length of the Gediz Graben and across the graben structures of the Aegean Region during the secondary event analysis. A secondary-event, de-clustering analysis was performed based on temporospatial windows proposed by Gardner and Knopoff (1974) in order to ensure that the catalogue has a Poisson distribution which is used to represent the earthquake phenomenon in time domain, and also to ensure a mutual exclusiveness of the events (i.e., main shocks and pre- and after-shocks). It was observed during the analysis that there is a clear seismicity relation throughout the graben structure and across normal fault dominated, extensional regime grabens of the Aegean Region where after-shocks were observed up to a 50 km distance from main events. Furthermore, in order to ensure the catalogue completeness principle (Stepp, 1973), only events after 1964 were used in the final analysis (Atakan et al., 2002; Kalkan et al, 2009; Cambazoğlu et al., 2016). Thus, following de-clustering analysis and the time threshold of 1964, a total of 3358 events out of 9293 earthquakes with Mw>3.0 were used to generate the b-value map. The map was generated with a 0.001 decimal degree resolution and resampled to 30 m x 30 m resolution (Figure 9).

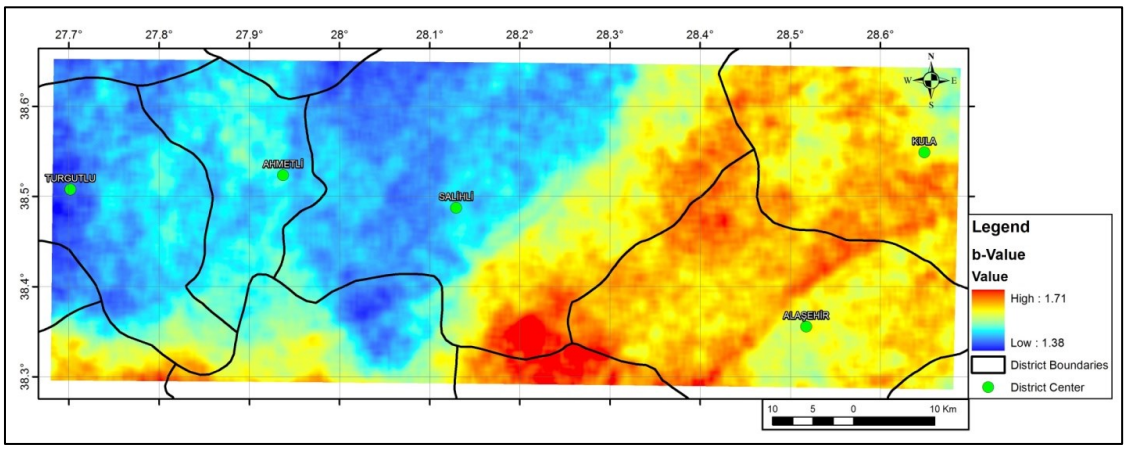

Figure 9. Gutenberg-Richter b-value map.

The final layer used for the assessment was the slope angle map generated from DEM created with a 30 m resolution by using digitized contours of the 1:25000 scale topographical maps. The slope values in the study area range between 0° and 55.3° with a mean of 10.4° and a standard deviation of 9.4°. The resultant slope angle map is reclassified into four discrete classes as: 1 for values lower than 10°, 0.5 for values between 10° and 20°, 0.25 for values between 20° and 30°, and 0 for values higher than 30° (Figure 10). The slope layer is included in the analysis with low importance as it is a parameter related with the accessibility which is not directly related with geothermal potential but rather with favorability.

The Normalized Difference Vegetation Index layer was generated by using Path: 180, Row: 33 Landsat 8 OLI&TIRS image acquired on June 20, 2016, courtesy of the U.S. Geological Survey (USGS-EROS, 2017). The NDVI layer is generated by using 30 m resolution Near-Infrared (NIR-band 5) and Red (RED-Band 4) bands of Landsat 8 image according to the NDVI = (NIR-RED)/(NIR+RED) relation which represents the density of green biomass with a data range between -1 and +1, where higher values indicate healthy vegetation (Figure 11). The NDVI layer is classified as a binary variable by using a threshold value of 0.353 (mean + standard deviation), indicating the healthy and dense vegetation above this threshold, are defined as '0' whereas the values lower than this threshold are defined as '1'. The NDVI layer was included in the analysis with the lowest importance as a land cover indicator in terms of favorability.

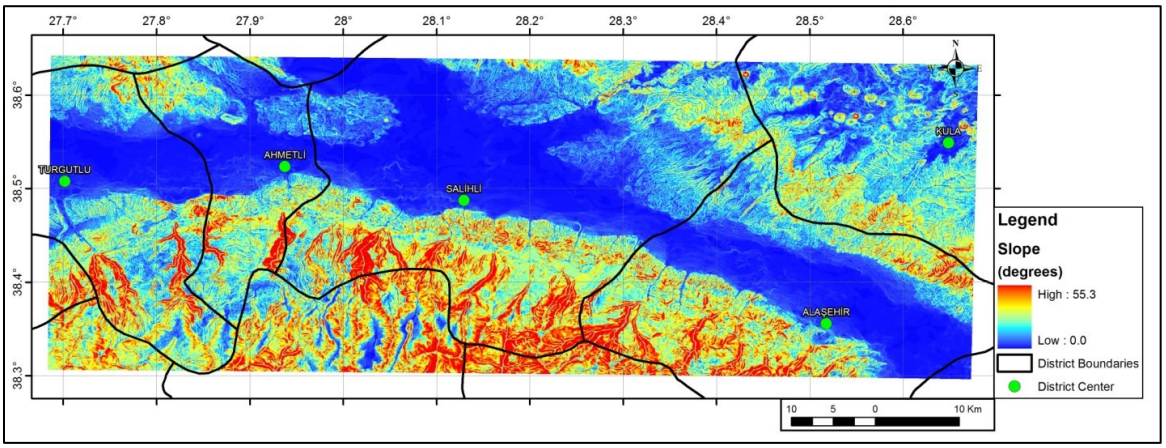

Figure 10. Slope map of the study area.

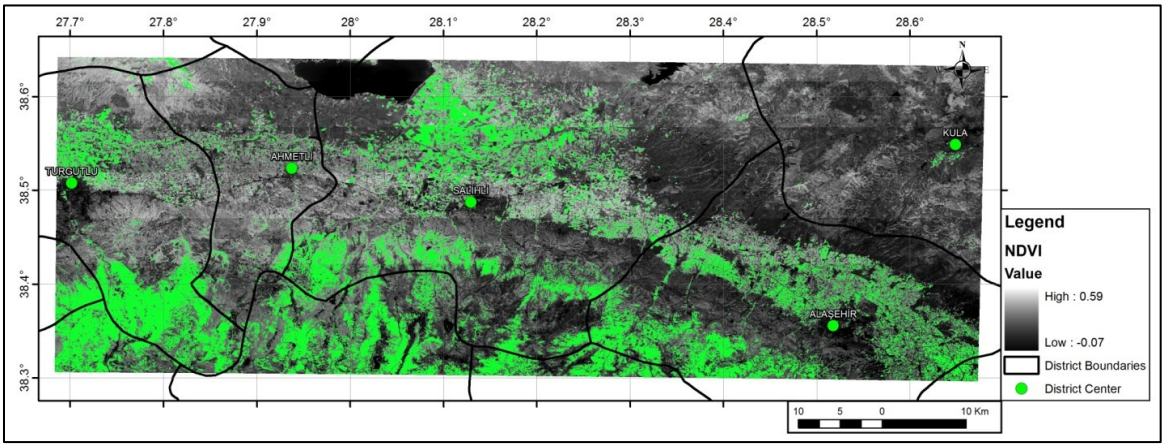

Figure 11. NDVI map with pixels above 0.353 threshold shown in green.

4. METHODOLOGY AND ANALYSES

In a geothermal project, a secondary thorough exploration stage is usually performed after initial reconnaissance and prior to well site selection in consideration of the high drilling costs. GIS has been proven to be a useful tool in detecting the spatial correlations between various types of data to aid in identifying potential zones (Bonham-Carter et al., 1988; Chung et al., 1992). Furthermore, MCDA techniques based on GIS serve as a powerful tool where the geographical data and the decision maker's preferences are integrated through a specified decision rule (Malczewski, 1999) and these techniques can be categorized into knowledge driven and data-driven methods (Bonham-Carter, 1994). Some examples of data driven methods are weight-of-evidence (Bonham-Carter et al., 1988; Coolbaugh et al., 2003; Coolbaugh and Bedell, 2006; Coolbaugh et al., 2007; Tufekci et al., 2010; Moghaddam et al., 2014), evidential belief function method (Carranza et al., 2008; Moghaddam et al., 2013), certainty factor based models (Li and Zhang, 2017). On the other hand, in knowledge driven methods, the relative importance of each criterion is subjectively determined by the judgment of experts. Index overlay (Prol-Ledesma, 2000; Noorollahi et al., 2008), weighted linear combination (Noorollahi et al., 2007; Yalcin and Kilic-Gul, 2017; Kiavarz and Jelokhani-Niaraki, 2017), fuzzy scheme models (Prol-Ledesma, 2000) and Boolean (Yousefi et al., 2007; Noorollahi et al., 2008; Yousefi et al., 2010) are some examples of this method in geothermal applications.

In this study, a knowledge driven ideal point methodology, namely, the Technique for Order Preference by Similarity to Ideal Solution (TOPSIS) (Jankowski and Ewart, 1996; Malczewski, 1996; Chen et al., 2001) has been employed. TOPSIS methodology has been implemented in many areas such as landfill site selection (Yal and Akgün, 2013, 2014), environmental assessment (Liu et al., 2006), and mineral mapping (Pazanda et al., 2012; Abedi and Norouzi, 2016), and it was used herein in order to produce a geothermal favorability map of Gediz Graben, Manisa, Turkey.

TOPSIS method, first introduced by Hwang and Yoon (1981), is based on selecting the best alternative with the shortest Euclidean distance from the ideal solution and farthest from the negative ideal solution (Malczewski and Rinner, 2015). The alternative with the highest closeness measure is selected (Zanakis et al., 1998). TOPSIS methodology was followed to generate the final favorability map by using a number of datasets. The datasets and the criteria constructed from these datasets along with their sources are given in Table 1. Each dataset was used to generate a criteria map and further weighted according to their relative importance.

For criteria weighting, the pairwise comparison method was used and a weight value was assigned to each criterion. The Pairwise Comparison (paired comparison) Method, developed by Saaty (1980), allows to determine the relative importance of an entity by comparing all entities in pairs. As a conventional geothermal system requires the existence of four major factors; i) a natural heat source, such as cooling magma, ii) an impervious cover rock, iii) a permeable reservoir and iv) consequently, sufficient fluid flow (Özgüler et al., 1983), the relative importance of the criteria layers was assigned accordingly (Cambazoğlu et al., 2019). Therefore, in this previous study by Cambazoğlu et al. (2019) the highest importance was given to the fault related criteria which are directly related with the fracture network generation (i.e., permeability) and heat transfer from the depth. Secondly, distance to hot spring locations was ranked which is a direct surface manifestation of geothermal occurrence. The distance to cap rock criteria was ranked third which is another requirement for geothermal presence. The next importance was given to the final geological parameter, namely, the distance to the graben center which is linked to the cap rock units and the asymmetrical character of the Gediz Graben. ASTER night-time surface temperature criterion was ranked following the primary geothermal indicators and is followed by the Gutenberg-Richter b-value, related with the seismo-tectonic activity of the region. The final two criteria, namely slope and NDVI is not directly related with geothermal occurrence and have significance in terms of land cover and accessibility, which is related with the well siting (i.e., favorability), and thus were assigned the least importance. Finally, the weight of fault related criterion is further divided into fault density and distance to fault according to a 0.6–0.4 weight ratio, respectively (Table 2).

In addition, a multi co-linearity analysis, where the tolerance is the percent of the variance in a given variable that cannot be explained by other variables and tolerance values close to 0 indicate high multi co-linearity and inflated regression coefficients (Norusis, 2004), was performed on each variable data set to avoid any major interdependency. The results of multi co-linearity analysis on variables (Table 3) have shown no co-linearity as the VIF (variance inflation factor) values were below 5 and tolerance values were above 0.2 (Menard, 1995; Rogerson, 2001).

The geothermal favorability map of the Gediz Graben based on this expert opinion ranking approach by a previous study (Cambazoğlu et al., 2019) have shown a success rate of 76% based on number of producing geothermal wells falling within the highest two favorability classes (80 out of 105) out of 6 classes divided based on equal area approach (Figure 12). In order to assess the success of this initial ranking, a bivariate correlation between each criteria layer and final favorability map was performed according to Pearson Correlation approach and each criteria layer was then re-ranked based on correlation coefficients (Table 2).

Table 2. Criteria layers, weights and ranks based on knowledge based and correlation based ranking as well as tolerance and variance inflation factors (VIF).

Criteria Layer	Knowledge Based Rank	Knowledge Based Weight	Bivariate Correlation Coefficient	Correlation Based Rank	Correlation Based Weight	Toler.	VIF
Fault density	1	0.22	.900	1	0.22	0.649	1.541
Distance to fault	1	0.14	.760	1	0.14	0.909	1.100
Distance to hot springs	3	0.23	.748	4	0.15	0.239	4.187
Cap rock	4	0.15	.475	5	0.10	0.659	1.517
Distance to graben center	5	0.10	.751	3	0.23	0.221	4.531
Night-time surface temperature	6	0.07	.071	8	0.03	0.901	1.110
b-value	7	0.04	.094	7	0.04	0.911	1.098
Slope angle	8	0.03	-.201	6	0.07	0.712	1.405
NDVI	9	0.02	-.033	9	0.02	0.895	1.118

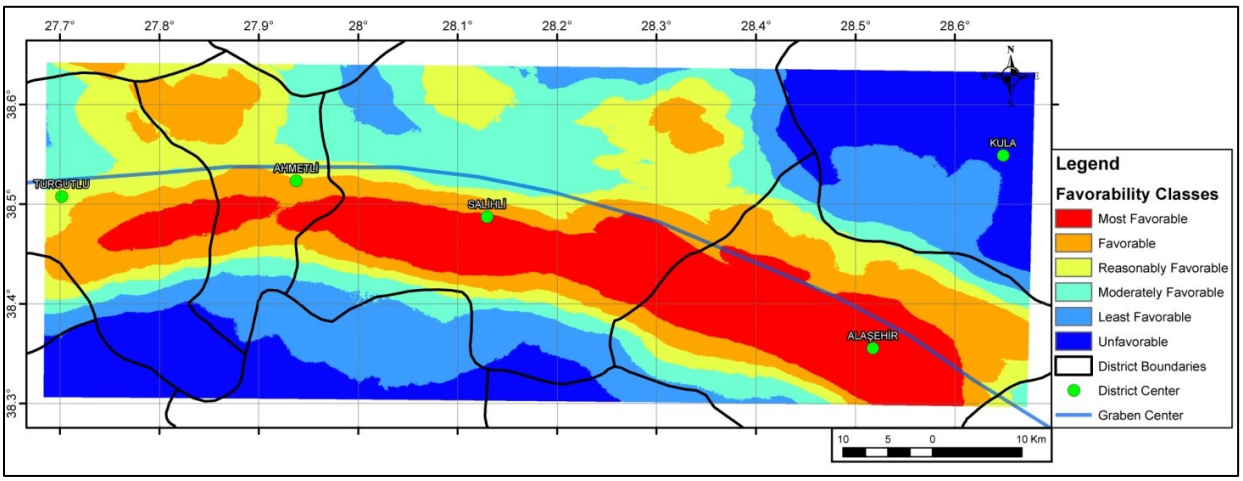

Figure 12. Geothermal favorability map of the Gediz Graben based on expert opinion (knowledge based) criteria ranking (Cambazoğlu et al., 2019).

The Pearson correlation coefficient (Pearson, 1895) was used to identify the degree of linear correlation between dependent and explanatory variables. The coefficient ranges between -1 and 1 where the sign indicates negative or positive correlation respectively and the value of the coefficient indicates the degree of correlation. Therefore, the result of a bivariate, Pearson correlation shows the degree of linear dependence between two variables. The bivariate normal distribution assumption can be replaced with the assumption that one of the variables has normal distribution and the two variables are independent (Hogg and Craig, 1978). Hence, prior to performing bivariate correlation, each dataset was individually inspected and the necessary transformations were performed. The correlation coefficients of the bivariate correlation have shown that the primary criteria layers, namely fault density and distance, distance to graben center, distance to hot springs and distance to cap rock units have significant correlation with the favorability map whereas the secondary criteria layers, namely slope angle, b-value, night-time surface temperature and NDVI, have low to very low correlation. Therefore, the TOPSIS analysis was repeated based on this new relative ranking and weight assignment (Table 2).

4. RESULTS AND DISCUSSION

According to the results of bivariate Pearson correlation, the ranking of the criteria layers was changed where fault density and distance to fault layers remained the highest and NDVI remained the lowest ranked layer. As can be seen from Table 2, the criteria layers can be divided into two groups where fault, hot spring and geology related layers can be considered as primary and have significant correlation. On the other hand, the b-value, slope, night-time surface temperature and NDVI layers have low correlation with the favorability map. The most significant result of the bivariate correlation is that the correlation coefficient of distance to cap rock unit layer is 0.475, which indicates moderate correlation. This result is probably due to the fact that approximately 57% of the entire study area is covered by cap rock units which may have caused this moderate correlation due to lack of variation. Along with this, it can be observed that the three lowest ranked layers have considerably insignificant correlation with the favorability map and the slope angle layer have low correlation.

Therefore, TOPSIS analysis was repeated based on this new ranking according to according to bivariate correlation results. In order to allow comparison of two favorability maps based on knowledge based and bivariate correlation based rankings, the correlation based favorability map were also divided into 6 classes with equal area approach (Figure 13). The resultant map was compared with the locations of the producing wells, where 75% of the wells (79 out of 105) corresponded to the highest two favorability classes and again, no wells fell within the least favorable and unfavorable classes of the final map (Table 3).

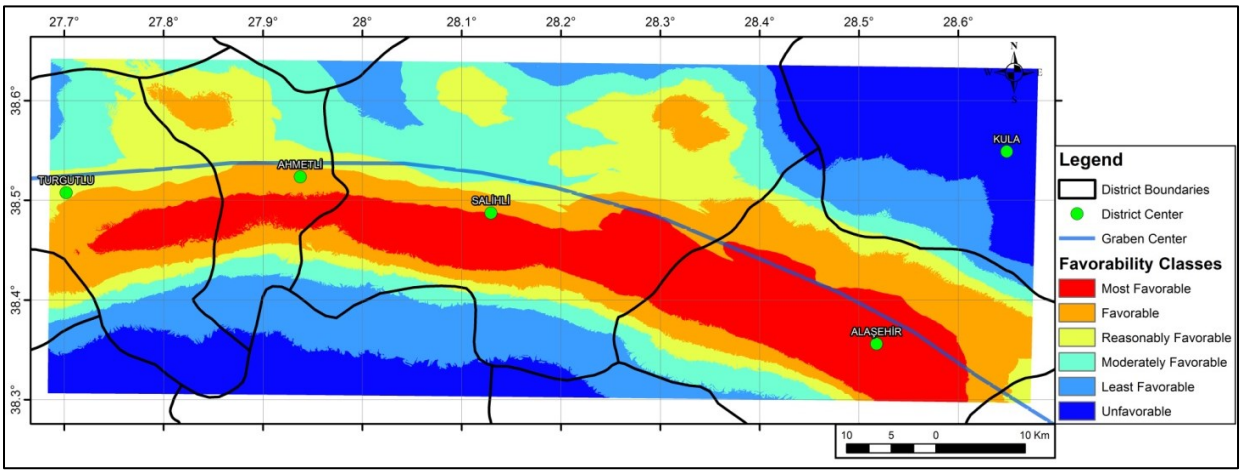

Figure 13. Geothermal favorability map of the Gediz Graben based on results of bivariate correlation criteria ranking.

Table 3. The number and percent of wells corresponding to each class.

Class	Category	According to Knowledge Based Ranking		According to Bivariate Correlation Based Ranking	
		Number of Wells	%	Number of Wells	%
6	Most favorable	51	48.57	52	49.52
5	Favorable	29	27.62	27	25.71
4	Reasonably favorable	17	16.19	17	16.19
3	Moderately favorable	8	7.62	9	8.57
2	Least favorable	0	0.00	0	0.00
1	Unfavorable	0	0.00	0	0.00

5. CONCLUSION

In this study, a favorability map of the Gediz Graben region generated previously based on knowledge based ranking approach of the criteria layers was correlated with the criteria layers according to bivariate Pearson Correlation. Each layer, then, was re-ranked according to results of the correlation and a new favorability map was generated by applying the same TOPSIS methodology with the new weight values for criteria layers. It was observed that the ranking of criteria layers can be divided into two as primary and secondary variables where the primary criteria include geothermal related layers being fault density, distance to fault, distance to hot springs, distance to graben center and distance to cap rock units which have shown strong correlation with the favorability map with the exception of distance to cap rock units layer. The distance to cap rock units layer have shown moderate correlation with the favorability map which is considered to be a result of large areal coverage of the units within the study area with 57% coverage. These primary variables were ranked highest in both knowledge based and correlation based rankings. The remaining criteria layers night-time surface temperature, b-value and NDVI layers shown very low, insignificant correlation while slope layer have presented low correlation with the favorability map and can be considered as secondary variables.

Therefore, the TOPSIS analysis was repeated with the new correlation result based on ranking and corresponding weights. It can be seen that the two favorability maps are similar in the main graben region. The success rate of the two favorability maps, namely knowledge based and correlation based maps, according to number of producing wells falling within each favorability class have shown that the two maps have presented very similar success rate (Table 3). Out of 105 known producing wells, the number of wells falling within the highest two favorability classes were 80 and 79 for the favorability maps generated according to knowledge based and correlation based ranking approaches, respectively. In order to further compare the two favorability maps, correlation based map was extracted from the knowledge based map. The resultant map have shown that 83.64% of the favorability areas remained unchanged whereas favorability class of 8.22% of the cells have decreased to one lower class and favorability class of 8.12% of the cells have increased to one higher class. As a conclusion, the result of the bivariate correlation based favorability map was, although by a small amount, lower than the knowledge based favorability map.

REFERENCES

Abedi, M., Norouzi, G.H.: A general framework of TOPSIS method for integration of airborne geophysics, satellite imagery, geochemical and geological data, *International Journal of Applied Earth Observation and Geoinformation* 46, (2016), 31-44.

Akkuş, İ., Akıllı, H., Ceyhan, S., Dilemre, A. and Tekin, Z.: Geothermal Resource Inventory of Turkey, *MTA General Directorate of Mineral Research and Exploration Press*, Envanter Serisi, (In Turkish) 201, (2005).

Arslan, S., Akın, U., and Alaca, A.: Assessment of Crustal Structure of Turkey with Gravity Data, *MTA Journal*, 140, (In Turkish), (2010), 57-73.

Atakan, K., Ojeda, A., Meghraoui, M., Barka, A., Erdik, M. and Bodare, A.: Seismic hazard in Istanbul following the 17 August 1999 Izmit and 12 November 1999 Duzce earthquakes, *Bull. Seismol. Soc. Am.*, 92(1), (2002), 466–82.

Bonham-Carter, G.F., Agterberg, F.P., Wright, D.F.: Integration of geological datasets for gold exploration in Nova Scotia, *Photogrammetry and Remote Sensing*, 54, (1988), 1585-1592.

Bonham-Carter, G.F.: Geographical Information Systems for Geoscientists: Modeling with GIS. Computer Methods in the Geosciences 13, *Pergamon*, New York, (1994), 398 pp.

Bozkurt, E., Sözbilir, H.: Tectonic evolution of the Gediz Graben: Field evidence for an episodic, two-stage extension in western Turkey*, Geol. Mag*., 141, (2004), 63-79.

Cambazoğlu, S., Koçkar, M.K. and Akgün, H.,: A generalized seismic source model for the Eastern Marmara Region along the segments of the North Anatolian Fault System, *Soil Dynamics and Earthquake Engineering*, 88, (2016) 412-426.

Cambazoğlu, S., Yal, G.P., Eker, A.M., Şen, O. and Akgün, H.: "Geothermal Resource Assessment of the Gediz Graben Utilizing TOPSIS Methodology, *Geothermics*, 80, (2019), 92- 102.

Carranza, E.J.M., Wibowo, H., Barritt, S.D., Sumintadireja, P.: Spatial data analysis and integration for regional-scale geothermal potential mapping West Java, Indonesia, *Geothermics*, 37 (3), (2008), 267–299.

Chen, K., Blong, R., Jacobson, C.: MCE-RISK: integrating multicriteria evaluation and GIS for risk decision-making in natural hazards, *Environmental Modelling and Software*, 16(4), (2001), 387–397.

Chung, C.F., Jeoerson, C.W., Singer, D.A.: A quantitative link among mineral deposit modeling, geoscience mapping, and exploration-resource assessment, *Economic Geology*, 87, (1992), 194–197.

Coolbaugh, M., Sawatzky, D., Oppliger, G., Minor, T., Raines, G., Shevenell, L., Blewitt, G., Louie, J.,: Geothermal GIS coverage of the Great Basin, USA: defining regional controls and favorable exploration terrains, *Transactions – Geothermal Resources Council*, (2003), 9–14.

Coolbaugh, M.F., Bedell, R.: A simplification of weights of evidence using a density function and fuzzy distributions, geothermal systems, In: Harris, J.R. (Ed.), *GIS for the Earth Sciences. Geological Assoc. of Canada, Special Pub*, 44, (2006), 115-130.

Coolbaugh, M. F., Raines, G. L., and Zehner, E.: Assessment of exploration bias in data-driven predictive models and the estimation of undiscovered resources, *Nat. Resour. Res.*, 10 (2), (2007), 199–207.

Çiftçi, N.B., Bozkurt, E.: Pattern of normal faulting in the Gediz Graben, SW Turkey, *Tectonophysics*, 473, (2009), 234-260.

Çiftçi, N.B., Bozkurt, E.: Structural evolution of the Gediz Graben, SW Turkey: temporal and spatial variation of the graben basin, *Basin Research*, 22, (2010), 846–873.

Duman, T.Y., Emre, Ö., Doğan, A., Özalp, T., Elmacı, H.: 1:250.000 Scale Active Fault Maps of Turkey, *General Directorate of Mineral Research and Exploration (MTA)*, Ankara-Turkey, (2011).

Eneva, M., Coolbaugh, M.: Importance of elevation and temperature inversions for the interpretation of thermal infrared satellite images used in geothermal exploration, *Geothermal Resources Council Transactions*, 33, (2009), 467–470.

Gardner, J.K., Knopoff, L.: Is the Sequence of Earthquakes in Southern California, with Aftershocks Removed, Poissonian?, *Bulletin of the Seismological Society of America*, 64, (1974), 1363-1367.

General Command of Mapping: 1:25,000 Scale Topographic Maps of Turkey, Ankara (2000).

Gessner, K., Gallardo, L.A., Markwitz, V., Ring, U., Thomson, S.N.: What caused the denudation of the Menderes Massif: review of crustal evolution, lithosphere structure, and dynamic topography in southwest Turkey, *Gondwana Research*, 24, (2013), 243–274.

Gillespie, A., Rokugawa, S., Matsunaga, T., Cothern, J. S., Hook, S., Kahle, A. B.: A Temperature And Emissivity Separation Algorithm for Advanced Spaceborne Thermal Emission and Reflection Radiometer (ASTER) Images, *IEEE Transactions on Geoscience and Remote Sensing*, 36, (1998) 1113−1126.

Gutiérrez, F.J., Lemus, M., Parada, M.A., Benavente, O.M., Aguilera, F.A.: Contribution of ground surface altitude difference to thermal anomaly detection using satellite images: Application to volcanic/geothermal complexes in the Andes of Central Chile, *Journal of Volcanology and Geothermal Research*, 237, (2012), 69-80.

Gutenberg, B., Richter, C.F.: Seismicity of the Earth and Associated Phenomenon, *Princeton University Press*, Princeton, New York, (1949).

Hook, S.J., Gabell, A.R., Green, A.A., Kealy, P.S.: A comparison of techniques for extracting emissivity information from thermal infrared data for geologic studies. *Remote Sensing of Environment*, 42, (1992), 123-135.

Hwang C.L., Yoon K.: Multiple attribute decision making: methods and applications : a state-of-the-art survey, *Springer-Verlag*, New York, 259 pp, (1981).

Jankowski, P., Ewart, G.: Spatial decision support system for health practitioners: selecting a location of rural health practice, *Geographical Systems*, 3(2), (1996), 279-299.

Kalkan E, Gulkan P, Yilmaz N, Celebi M.: Reassessment of Probabilistic seismic hazard in the Marmara Region, *Bull Seismol. Soc. Am.*, 99(4), (2009), 2127–2146.

Kiavarz, M., Jelokhani-Niaraki, M.: Geothermal prospectivity mapping using GIS-based Ordered Weighted Averaging approach: A case study in Japan's Akita and Iwate provinces, *Geothermics,* 70, (2017), 295-304.

Klingel, E., Tavlan, M., Ozcetin, K., de Wijkerslooth, C.: Geothermal Exploration Where Innovative Meets Classic Geothermal Exploration in Western Anatolia, *Proceedings*, World Geothermal Congress Melbourne, Australia (2015).

KOERI: Earthquake Catalogue (http://www.koeri.boun.edu.tr/sismo/2/earthquake-catalog/, access date: January, 30 .2017 (2017).

Li, J., Zhang, Z.: GIS-supported certainty factor (CF) models for assessment of geothermal potential: A case study of Tengchong County, southwest China, *Energy*, 140, (2017), 552-565.

Liu, C., Frazier, P., Kumar, L., Macgregor, C., Blake, N.: Catchment-wide wetland assessment and prioritization using the multi-criteria decision-making method TOPSIS, *Environmental Management*, 32(2), (2006), 316–326.

Malczewski, J.: A GIS-based approach to multiple criteria group decision-making, *International Journal of Geographical Information Systems*, 10, (1996), 955–971.

Malczewski, J.: GIS and Multicriteria Decision Analysis, *John Wiley & Sons*, 387 pp, (1999).

Malczewski, J., Rinner, C.: Multicriteria Decision Analysis in Geographic Information Science, *Springer*, New York, 331 pp, (2015).

Menard, S.: Applied Logistic Regression Analysis, *Sage University Series on Quantitative Applications in the Social Sciences*, Thousand Oaks, CA: Sage, (1995).

Moghaddam, M.K., Noorollahi, Y., Samadzadegan, M.K., Sharifi, M.A., Itoi, R.: Spatial data analysis for exploration of regional scale geothermal resources, *Geothermics*, 266, (2013) 69-83.

Moghaddam, M.K., Samadzadegan, F., Noorollahi, Y., Sharifi, M.A., Itoi, R.: Spatial analysis and multi-criteria decision making for regional-scale geothermal favorability map, *Geothermics* 50, (2014), 189-201.

MTA: 1/500.000 Scale Geological Maps, General Directorate of Mineral Research and Exploration (MTA). Turkey, (2002).

NASA LP DAAC: Aster Level 1 Precision Terrain Corrected Registered At-Sensor Radiance V003, NASA EOSDIS Land Processes DAAC. USGS Earth Resources Observation and Science (EROS) Center, Sioux Falls, South Dakota (https://lpdaac.usgs.gov), Doi:10.5067/Aster/Ast_L1t.003, (Http://Earthexplorer.Usgs.Gov/), Accessed On January 15, 2017, (2017).

Noorollahi, Y., Itoi, R., Fujii, H., Tanaka, T.: GIS model for geothermal resource exploration in Akita and Iwate prefectures, northern Japan, *Geothermics*, 33, (2007), 1008-1021.

Noorollahi, Y., Itoi, R., Fujii, H., Tanaka, T.: GIS integration model for geothermal exploration and well siting, *Geothermics*, 37, (2008), 107–131.

Norusis, M.: SPSS 13.0 guide to data analysis, *Prentice Hall, Inc.*, Upper Saddle-River, NJ, (2004), 13 pp.

Özgüler, M.E., Turgay, C., Şahin, H.: Geophysical studies in Denizli geothermal field, *MTA J.* 99-100, (1983), 129–142 (in Turkish).

Pazanda, K., Hezarkhani, A., Mohammad, A.: Using TOPSIS approaches for predictive porphyry Cu potential mapping: A case study in Ahar-Arasbaran area (NW, Iran), *Computers and Geosciences*, 49, (2012), 62-71.

Pearson, K.: Notes on Regression and Inheritance in the Case of Two Parents, *Proceedings*, the Royal Society of London, 58, (1895), 240–242

Prol-Ledesma, R.: Evaluation of the reconnaissance results in geothermal exploration using GIS, *Geothermics*, 29 (1), (2000), 83–103.

Rogerson, P. A.: Statistical Methods for Geography, *London: Sage*, (2001).

Saaty, T.L.: The analytic hierarchy process, *McGraw-Hill, New York*, (1980).

Shah, S.T.: Stress Tensor Inversion From Focal Mechanism Solutions and Earthquake Probability Analysis of Western Anatolia, Turkey, Doctoral Dissertation, *Middle East Technical University*, (2015).

Sözbilir, H.: Geometry and origin of folding in the Neogene sediments of the Gediz Graben, western Anatolia, Turkey, *Geodin. Act.*, 15, (2002), 277-288.

Stepp, J. C.: Analysis of Completeness of the Earthquake Sample in the Puget Sound area, In Contributions to Seismic Zoning: U.S. National Oceanic and Atmospheric Administration Technical Report, ERL 267-ESL 30 (edited by Harding, S. T.), (1973), 16-28.

Tufekci, N., Suzen, M.L., Gulec, N.: GIS based geothermal potential assessment: a case study from Western Anatolia, Turkey, *Energy*, 35 (1), (2010), 246–261.

USGS-EROS, Landsat 8 OLI/TIRS CI Level 1 Archive, addessed online: http://earthexplorer.usgs.gov (Accessed on 15 January 2017), (2017).

Wiemer, S.: A software package to analyze seismicity: ZMAP, *Seism. Res. Lett.*, 72, (2001), 373–382.

Yal, G.P., Akgün, H.: Landfill Site Selection Utilizing TOPSIS Methodology and Clay Liner Geotechnical Characterization: A Case Study for Ankara, Turkey, *Bulletin of Engineering Geology and the Environment*, 73(2), (2014), 369-388.

Yal, G.P., Akgün, H.: Landfill Site Selection and Landfill Liner Design for Ankara, Turkey, *Environ Earth Sci.* 70, (2013), 2729–2752.

Yalcin, M., Kilic Gul, F.: A GIS-based multi criteria decision analysis approach for exploring geothermal resources: Akarcay basin (Afyonkarahisar), Geothermics, 67, (2017), 18-28.

Yilmaz, Y., Genç, Ş.C., Gürer, F., Bozcu, M., Yilmaz, K., Karacik, Z., Altunkaynak, Ş., Elmas, A.: When did the western Anatolian grabens begin to develop? *Geological Society, London, Special Publications*, 173(1), (2000) 353-384.

Yilmazer, S., S. Pasvanoglu, Vural, S.: The relation of geothermal resources with young tectonics in the Gediz graben (West Anatolia, Turkey) and their hydrogeochemical analyses, In *Proceedings* World Geothermal Congress. pp. 1-10, (2010).

Yousefi, H., Ehara, S., Noorollahi, Y.: Geothermal potential site selection using GIS in Iran, *Proceedings*, 32nd Workshop on Geothermal Reservoir Engineering, Stanford University, Stanford, CA, (2007).

Yousefi, H., Noorollahi, Y., Ehara, S., Itoi, R., Yousefi, A., Fujimitsu, Y., Nishijima, J.,Sasaki, K.: Developing the geothermal resources map of Iran, *Geothermics*, 39, (2010), 140–151.

Zanakis, S. H., Solomon, A., Wishart, N., Dublish, S.: Multi-attribute decision making: A simulation comparison of select methods, *European Journal of Operational Research*, 107(3), (1998), 507-529.